Observed and Calculated Infrared Spectra of $Pd(H_2)_{1,2,3}$ Complexes and Palladium Hydrides in Solid Argon and Neon

Lester Andrews,*,†,‡ Xuefeng Wang,† Mohammad Esmaïl Alikhani,‡ and Laurent Manceron‡

Chemistry Department, University of Virginia, Charlottesville, Virginia 22904-4319, and LADIR/Spectrochimie Moléculaire, UMR 7075, Université Pierre et Marie Curie, case courrier 49, 4 Place Jussieu, 75252 Paris Cedex 05, France

Received: October 10, 2000; In Final Form: January 9, 2001

Thermally evaporated and laser-ablated Pd atoms interact with H_2 in excess argon to form the side-bonded $Pd(H_2)$ complex, which is characterized by 2971, 1507, and 950 cm^{-1} fundamental frequencies. These infrared absorptions are assigned to $Pd(H_2)$ on the basis of the HD and D_2 shifts and DFT frequency calculations. Higher H_2 concentrations favor the $Pd(H_2)_{2,3}$ complexes, which exhibit 3038, 778 cm^{-1} and 2909, 730, 319 cm^{-1} fundamentals, respectively. These complexes involve electrostatic bonding owing to a small amount of charge reorganization. Higher Pd concentrations enhance absorptions due to a Pd--$Pd(H_2)$ complex and the stable $(PdH)_2$ molecule with no H−H bond. This work shows that one neutral Pd atom cannot insert into a H_2 molecule but that two Pd atoms dissociate molecular hydrogen with no activation energy. Laser ablation produces energetic Pd atoms which also form PdH, electrons which are captured to give PdH_2^-, and radiation which ionizes H and yields Ar_nH^+ in the matrix cage. Diatomic PdH also forms complexes with dihydrogen.

Introduction

Side bonding (η^2-coordination) of dihydrogen to metal centers is the first step in activation to form metal dihydrides. Hydrogen activation by metal centers is an important reaction in commercial processes and basic chemistry. Hydride complexes formed by the cleavage of H_2 are involved in a large number of reactions.[1] After preparation of the first stable dihydrogen complex, $W(CO)_3(PR_3)_2(\eta^2\text{-}H_2)$, by Kubas et al.,[2] a large number of transition metal complexes containing η^2-H_2 have been characterized, and their coordination chemistry and role in reduction processes have been reviewed.[3−12] A very recent investigation of Ru, CO, and H_2 in solid argon has identified both the $Ru(H_2)CO$ complex and the $RuH_2(CO)_2$ dihydride from infrared spectra and density functional calculations.[13]

The electronic properties of a metal center that will favor η^2-coordination as opposed to insertion to give the metal dihydride are of fundamental importance. A recent density functional theory (DFT) investigation by Morokuma et al.[14] found that platinium insertion is spontaneous with PtH_2 more stable by 47 kcal/mol than ground state atomic Pt and molecular H_2, but palladium complexation is favored as $Pd(H_2)$ is 16 kcal/mol more stable than atomic Pd and H_2. This result is in agreement with earlier calculations by Balasubramanian et al.[15,16] and with matrix isolation investigations by the Ozin and Weltner groups,[17,18] which reported spectra of PtH_2 and $Pd(H_2)$. The latter work describes the only experimental evidence to date for a naked metal−η^2-H_2 complex, namely the symmetric Pd−(H_2) stretching fundamental in solid krypton and xenon, but also claims formation of the η^1-H_2 (end bonded) complex as well. The $Pd(H_2)$ complex has been the subject of many theoretical investigations[19−22] and is described in a recent review.[23] A brief communication of our thermal and laser-ablation investigation has been published.[24]

Since the $Pd(H_2)$ complex is unique, it is fundamentally important to have the complete infrared spectrum and a theoretical model of the vibrational spectrum. We report here a complementary thermal-evaporation and laser-ablation matrix infrared and DFT pseudopotential investigation of the Pd/H_2 system. In addition to $Pd(H_2)$, we find evidence for $Pd(H_2)_2$, $Pd(H_2)_3$, Pd--$Pd(H_2)$, and $(PdH)_2$, which are formed in spontaneous reactions of Pd and H_2. Although one Pd atom cannot activate dihydrogen, two Pd atoms break the dihydrogen bond in the cold matrix to form the open ring $(PdH)_2$. Laser-ablation experiments also produce PdH and the $HPdH^-$ anion.

Experimental and Theoretical Methods

The experimental methods and apparatus employed in each laboratory for Pd atom reactions have been described in previous publications.[24−26] The laser-ablation technique as applied gives a lower mass flow of Pd atoms, but these atoms contain excess energy and some Pd cations and electrons as well as ultraviolet photons are also produced. For median conditions in both laboratories, a 5-fold higher metal atom concentration is typical of the thermal-evaporation experiment, which produces no ions and only orange-infrared radiation. Matrix-isolation experiments were performed for Pd atoms and H_2 in excess argon frozen on 7 and 9 K substrates and excess neon on a 4 K cesium iodide window. Infrared spectra were recorded, samples were annealed and irradiated, and more spectra were recorded.

DFT calculations were performed using the Gaussian 98 program system,[27] B3LYP and BPW91 density functionals,[28,29] 6-311+G(d, p), 6-311+G(2d,2p), and 6-311++G(2d,2p) basis sets for H,[30] and LANL2DZ and SDD pseudopotentials (18 valence electrons) for Pd.[31,32] Geometries were fully optimized, and the vibrational frequencies were computed analytically from second derivatives.

* To whom correspondence should be addressed at the University of Virginia. E-mail: lsa@virginia.edu.
† University of Virginia.
‡ Université Pierre et Marie Curie.

10.1021/jp003721t CCC: $20.00
Published on Web 03/06/2001

TABLE 1: Infrared Absorptions (cm^{-1}) Observed in Thermal-Evaporation and Laser-Ablation Pd Atom Matrix-Isolation Experiments with H_2 in Excess Argon Condensed at 9 and 7 K

H_2	HD	D_2	$H_2 + D_2$	identification
3038	2639	2160	3034[e]	B, $Pd(H_2)_2$
2971.4[a]	2334	2169, 1916[d]		A, $Pd(H_2)$, $\nu_1(a_1)$
2957.5				A, $Pd(H_2)$ site
2909	2545	2070	2897	C, $Pd(H_2)_3$
2858	2722	2061		E, $(PdH)_2$, $a_g + b_{2u}$
2401.8[b,d]				A, $Pd(H_2)$, $3\nu_2$
1952.8[c]	1952.8, 1403.5	1403.5		PdH
1900.8[c]	1899.0, 1368.2	1366.4	1897.9, 1369.2	$(H_2)-PdH$
1831.7[c]	1826.3, -	1315.5	1325.4, 1316.0	$(H_2)_x-PdH$
	1479.5			$PdHD^-$
	1431.5			E, Pd(HD)Pd, a_1
1507.5[b]	1305.6	1098.0		A, $Pd(H_2)$, $\nu_3(b_1)$
	1297.8			Pd--$Pd(H_2)$
1395, 1380		979		E, $(PdH)_2$
1347.7	1329.8	950.2		E, $(PdH)_2$, b_{2u}
	951.5			E, $(PdH)_2$, b_{2u}
	1172.0			B, $Pd(HD)_2$
	1105.5			C, $Pd(HD)_3$
1247.0[c]	981.8	908.5		PdH_2^-
954.4				A, $Pd(H_2)$ site
950.0	804.1	714.4		A, $Pd(H_2)$, ν_2 (a_1)
929.3, 927.6				D, Pd--$Pd(H_2)$ site
922.8	795.5	704.4		D, Pd--$Pd(H_2)$
920.7	793.9	702.8		D, Pd--$Pd(H_2)$ site
903.4[c]	903.4, 634.4	634.4		Ar_nH^+, Ar_nD^+
778.0	649.6	585.7	844, 624	B, $Pd(H_2)_2$
730.1	618.3, 587.7, 585.9	549.4	756, 564	C, $Pd(H_2)_3$
319.5	274.9, 266.3, 259.1	236.6	316.5, 269.5, 293.6, 236.6	C, $Pd(H_2)_3$

[a] Relative integrated intensities 2971.4(16), 2401.8(2) 1507.5(1), 954.4, and 950.0(360). [b] Bands observed only in thermal experiments. [c] Band observed only in laser ablation experiments. [d] Tentatively assigned to a Fermi resonance between $\nu_1(a_1)$ and $3\nu_2(a_1)$. [e] New bands observed only with the $H_2 + D_2$ mixture.

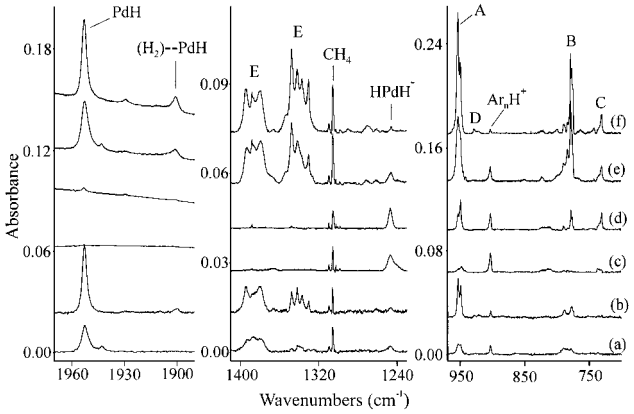

Figure 1. Infrared spectra in the 1970−1890, 1410−1230, and 970−700 cm^{-1} regions for laser-ablated Pd atoms codeposited with H_2 in excess argon: (a) 0.2% H_2 in argon deposited at 7 K for 80 min ; (b) after annealing to 30 K ; (c) 2% H_2 in argon deposited at 4 K for 60 min ; (d) after annealing to 20 K ; (e) 2% H_2 in argon deposited at 7 K for 80 min; (f) after annealing to 30 K.

Results

Observations from laser-ablation and thermal-evaporation experiments and product structures and frequencies from DFT calculations will be presented.

Laser Ablation. Investigations were done with low-energy (1−5 mJ/pulse) 1064 nm laser-ablated Pd (Johnson-Matthey) and low concentrations (0.2, 1, 2, and 6%) of H_2, HD, D_2, and $H_2 + D_2$ in solid argon on a 7 K CsI window.[26] Infrared spectra are shown in Figure 1, and product bands are listed in Table 1. Several product absorptions are unique to the laser-ablation experiments: the 1952.8 cm^{-1} band, which is due to PdH, and associated satellite features at 1900.8 and 1831.7 cm^{-1}, a new weak photosensitive 1247.0 cm^{-1} band, and the 903.4 cm^{-1} absorption, which arises from the Ar_nH^+ species,[33,34] are common to all laser-ablation experiments with H_2 present. The major bands at 954, 950, and 778.0 cm^{-1} (labeled A and B) and a weak 730.1 cm^{-1} band (noted C) increase on annealing. Other bands at 1395 and 1347.7 cm^{-1} (labeled E) increase, and weak bands appear at 929.3 and 922.8 cm^{-1} on annealing (labeled D) and disappear on photolysis. Figure 1 also contrasts a 2% H_2 sample in argon deposited on a 4 K substrate: there is very little effect on annealing to 10 K but substantial growth of the A−C bands on annealing to 20 K and an increase in relative intensity of the 1247.0 cm^{-1} band on deposition. In addition $\lambda > 470$ nm irradiation had no effect but $\lambda > 240$ nm irradiation virtually destroyed the 1247.0 cm^{-1} band and reduced the 903.4 cm^{-1} absorption to 40% of its initial absorbance. A very weak E band appeared on 20 K annealing, but no D band was detected. The A−E bands are common with thermal Pd experiments.[24]

Deuterium isotopic counterparts exhibit the same annealing and photolysis behavior, and the shifted frequencies are also listed in Table 1. Figure 2 shows the relevant spectral region. The photosensitive band at 908.5 cm^{-1} is much stronger than the H_2 counterpart at 1247.0 cm^{-1}. Annealing to 20 K increases the A, B, C and E bands but not the 908.5 and 634.4 cm^{-1} (Ar_nD^+)[33,34] features. Irradiation markedly diminishes the latter bands; however, annealing to 30 K increases the former bands, but not the latter bands, and produces a weak D band. A series of experiments with 2% D_2 and laser energy reduced by one and two 10% neutral-density filters reveal constant relative intensities for the A−C bands and suggest that these absorbers contain a common Pd atom stoichiometry. The new 908.5 and 634.4 cm^{-1} bands were favored relative to the 714.4 cm^{-1} band with decreasing laser power. Irradiation ($\lambda > 380$ nm) reduced the 634.4 cm^{-1} band to 70% of the original intensity and did not alter the 908.5 cm^{-1} band, but $\lambda > 290$ nm reduced the

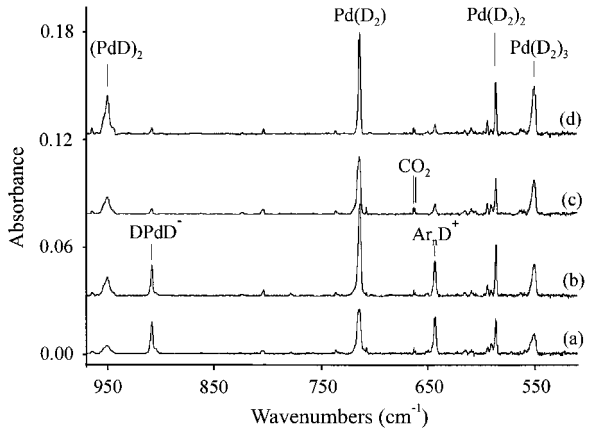

Figure 2. Infrared spectra in the 970−530 cm^{-1} region for laser-ablated Pd atoms codeposited with D_2 in excess argon: (a) 2% D_2 in argon deposited at 7 K for 80 min ; (b) after annealing to 20 K ; (c) after broad-band photolysis for 20 min; (d) after annealing to 30 K.

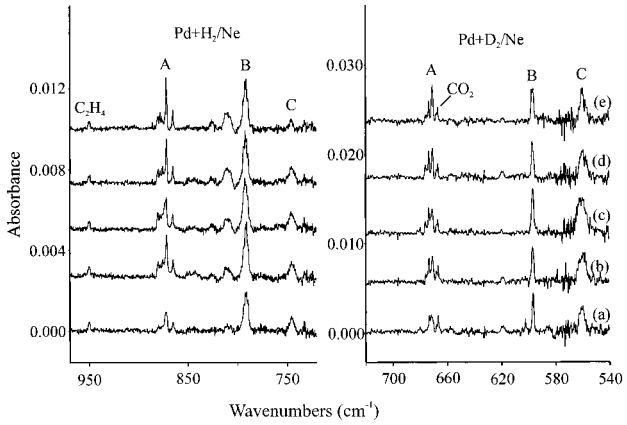

Figure 3. Infrared spectra in the 970−720 and 720−540 cm^{-1} regions for laser-ablated Pd atoms codeposited with H_2 and with D_2 in excess neon, respectively: (a) 1% H_2 in neon and 1% D_2 in neon, respectively, codeposited for 40 min; (b) after annealing to 6 K; (c) after broad-band photolysis for 20 min; (d) after annealing to 8 K; (e) after annealing to 10 K.

634.4 cm^{-1} band to 60% and the 908.5 cm^{-1} band to 80% and $\lambda > 240$ nm decreased these absorptions to 30 and 20% of their original intensities. Doping with CCl_4 was employed to provide an extra electron trap.[26] Adding 0.2% CCl_4 with 2% D_2 in a Pd experiment gave essentially the same 714.4 cm^{-1} band intensity as an identical laser power experiment done first with no CCl_4 additive, but the 908.5 cm^{-1} band was not present and the 634.4 cm^{-1} band intensity was increased 6-fold. Adding only 0.03% CCl_4 with 2% D_2 again gave the same A−C band intensities, double the 634.4 cm^{-1} absorption, but no 908.5 cm^{-1} band was detected. Experiments with HD gave counterparts of the strong A−E bands as listed in Table 1 and new 1479.5 and 981.8 cm^{-1} counterparts for the photosensitive species. Finally, a weak, sharp band at 2209.6 cm^{-1} observed in all of these experiments is due to PdNN;[35] however, PdO_2 (at 1023.0 cm^{-1})[36] was detected in only the most dilute hydrogen experiments.

A complementary series of neon matrix experiments was done using laser ablation with lower laser energy than for argon. The spectra in Figure 3 for 1% H_2 are representative: note growth of the sharp 871.9 and 792.4 cm^{-1} bands on 6 K annealing and reduction of the 871.9 cm^{-1} band on broad-band photolysis followed by recovery on 8 and 10 K annealing. Changing the H_2 concentration from 0.5 to 1.0 to 2.0% increased the intensity of the 745.2 cm^{-1} band relative to the 871.8 and 792.4 cm^{-1} bands. An experiment with 5% H_2 gave much stronger 792.4

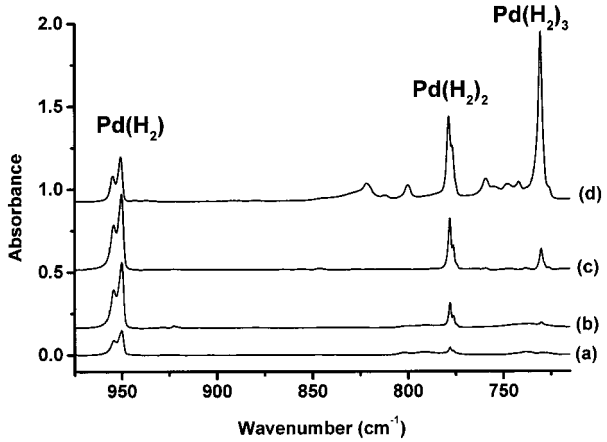

Figure 4. Infrared spectra of products formed by the reaction of thermal Pd atoms codeposited for 90 min with H_2 in excess argon at different concentrations: (a) $Pd/H_2/Ar = 0.5/2/100$; (b) $Pd/H_2/Ar = 0.6/4/100$; (c) $Pd/H_2/Ar = 0.3/8/100$; (d) $Pd/H_2/Ar = 0.3/24/100$.

TABLE 2: Infrared Absorptions (cm^{-1}) Observed in Laser-Ablated Pd Atom Matrix-Isolation Experiments with H_2 in Excess Neon at 4 K

H_2	HD	D_2	identification
1961.9	1961.9, 1409.8	1409.8	PdH, PdD
1958.5	1958.5, 1406.3	1406.3	PdH, PdD
1345.8	1329.7		$(PdH)_2$
	958.7	953.9	$(PdD)_2$
	1275.0		Pd(HD) site
	1273.3		Pd(HD)
	986.0	912.9	PdH_2^-
875.6	755.7	673.6	$Pd(H_2)$ site
871.8	752.0	670.9	$Pd(H_2)$
865.3			$Pd(H_2)$
792.4	663.3	597.5	$Pd(H_2)_2$
745.7	620	560.6	$Pd(H_2)_3$

and 745.7 cm^{-1} bands relative to the 871.8 and 865.3 cm^{-1} features. In addition, sharp weak bands were observed at 1961.9 and 1958.5 cm^{-1} and a broader 1345.8 cm^{-1} feature increased on annealing. The observed bands are collected in Table 2. The D_2 counterparts for the major absorptions are displaced to 670.9, 597.5, and 560.6 cm^{-1} as shown in Figure 3. In addition, sharp, weak bands were observed at 1409.8 and 1406.3 cm^{-1}, a new feature at 953.9 cm^{-1}, and a weak photosensitive band at 912.9 cm^{-1}. An experiment with HD gave the same sharp, weak bands, slight differences in bands now at 1329.7 and 958.7 cm^{-1}, and a weak photosensitive 986.0 cm^{-1} band. The major absorptions were found in intermediate positions at 752.0, 663.3, and 620 cm^{-1}. It is noteworthy that a weak 1275.0, 1273.3 cm^{-1} doublet tracked with the 755.7, 752.0 cm^{-1} doublet on annealing and photolysis: the former doublet was 10% as intense as the latter doublet in the HD experiment.

Several experiments were performed using D_2 as a matrix, and laser-ablated Pd into pure D_2 condensed at 4 K gave new absorptions at 1321.0, 952.6, and 556.5 cm^{-1}. Two experiments with 10% HD in D_2 gave the same bands plus a new 1830.4 cm^{-1} band 10% as intense as the 1321.0 cm^{-1} band; the same 1830.4 cm^{-1} band was observed with 5% H_2 in D_2.

Thermal Evaporation. Experiments were performed with Pd (0.1−0.6% as measured by quartz crystal microbalance) and H_2 (2, 4, 6, 8, 16, and 24%) in argon on a 9 K Ni-plated Cu substrate.[25] Figure 4 contrasts spectra in the 980−710 cm^{-1} region using different H_2 concentrations, and Figure 5 shows the effect of annealing and photolysis for an 8% H_2 sample. The actual concentration of H_2 trapped in the solid argon matrix is not known, but it is probably less than half of the concentra-

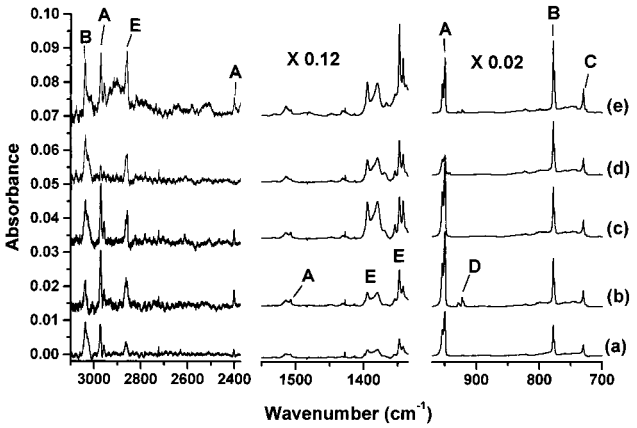

Figure 5. Infrared spectra of products formed by the reaction of thermal Pd atoms with H_2 in excess argon: (a) $Pd/H_2/Ar = 0.5/8/100$ codeposited at 9 K for 90 min; (b) after annealing to 19 K; (c) after 632 nm filter photolysis for 30 min; (d) after 365 nm filter photolysis for 80 min; (e) after annealing to 24 K. The absorbance scale was given for 3000−2400 cm^{-1} region; bands in the 1500−1400 cm^{-1} region have been reduced ×0.12 and in 1000−700 cm^{-1} region by ×0.02 so the indicated absorbance scale must be ×8 and ×50 for these regions, respectively. A weak, broad background absorption at 3030 cm^{-1} makes quantitative photometry difficult at this wavenumber.

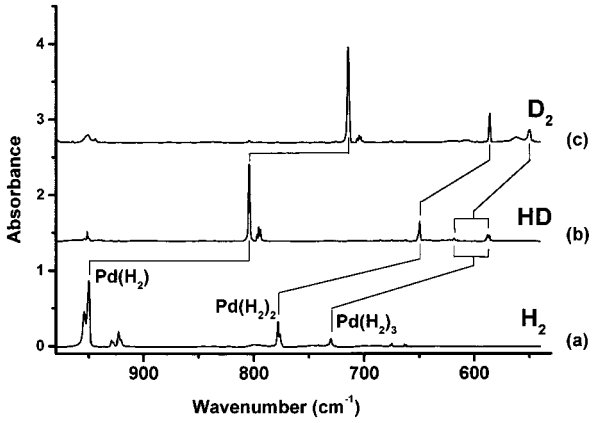

Figure 6. Infrared spectra in the 980−530 cm^{-1} region for thermal Pd atoms codeposited with 4% hydrogen isotopic samples in argon: (a) H_2; (b) HD; (c) D_2.

tion in the gas mixture. The 4260 cm^{-1} band attributed to $(H_2)_x$ clusters verifies that H_2 is trapped in these experiments.[37] It is clear that the B and C absorptions involve more H_2 submolecules than the A absorption and that both 730.1 cm^{-1} and a new 319.5 cm^{-1} band are due to species C. The D and E absorptions appear to have the same H_2 concentration dependence as the A absorption. At constant H_2 concentration the D and E bands are favored over A with increasing Pd concentration. An experiment performed with 4% H_2 and very low Pd concentration (<0.01%) as a test gave very weak A−C bands with the same relative intensities as in Figure 4b.

Similar experiments were done with 4% D_2 and HD, and spectra are compared in Figure 6. The spectra for HD with annealing in Figure 7 show the effect of symmetry lowering in the dihydrogen precursor; photolysis at 365 nm destroyed species D, markedly reduced species A, and slightly increased species E. In separate experiments, 632, 590, and 530 nm photolyses destroyed species D and increased only species E absorptions. Figure 8 contrasts mixed isotopic spectra for the strong 319.5 cm^{-1} absorption and demonstrates the involvement of three H_2 submolecules. Finally, the important H−H stretching region is illustrated in Figure 9 for H_2, HD, and D_2 samples.

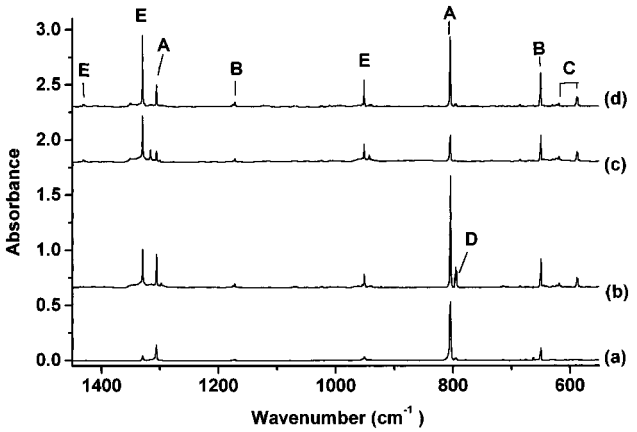

Figure 7. Infrared spectra in the 1450−550 cm^{-1} for Pd and HD in excess argon: (a) $Pd/HD/Ar = 0.3/4/100$ codeposited for 90 min at 9 K; (b) after annealing to 22 K; (c) after photolysis at 365 nm for 90 min; (d) after annealing to 29 K.

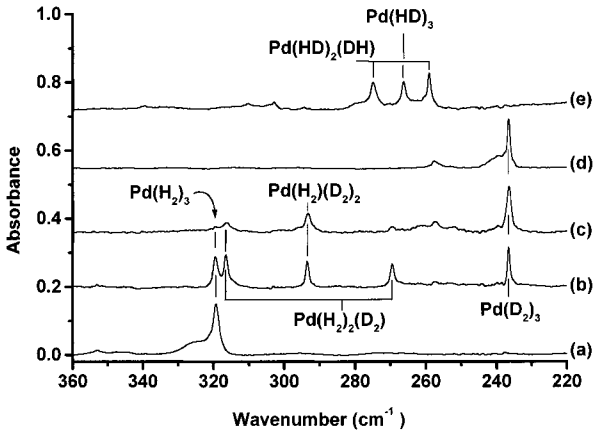

Figure 8. Infrared spectra in the 360−220 cm^{-1} region for Pd atoms codeposited with isotopic hydrogen samples in excess argon for 90 min at 9 K: (a) $Pd/H_2/Ar = 0.6/4/100$ after annealing to 29 K; (b) $Pd/H_2/D_2/Ar = 0.3/4/2/100$ after annealing to 20 K; (c) $Pd/H_2/D_2/Ar = 0.3/2/6/100$ after annealing to 29 K; (d) $Pd/D_2/Ar = 0.3/4/100$ after annealing to 21 K; (e) $Pd/HD/Ar = 0.3/8/100$ after annealing to 33 K.

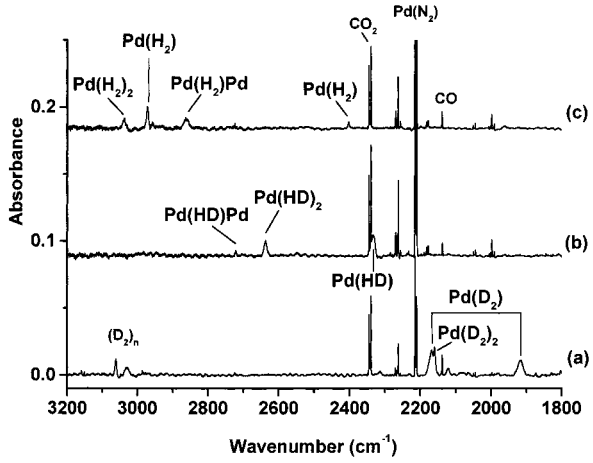

Figure 9. Infrared spectra in the 3200−1800 cm^{-1} region for palladium and hydrogen samples codeposited with excess argon for 90 min at 9 K: (a) $Pd/D_2/Ar = 0.3/8/100$; (b) $Pd/HD/Ar = 0.5/8/100$; (c) $Pd/H_2/Ar = 0.5/8/100$.

Calculations. DFT calculations for anticipated product molecules using different functionals and pseudopotentials are compared in Table 3 for PdH and $Pd(H_2)$. The PdH and PdD molecules are known experimentally (PdH fundamental 1945

TABLE 3: Frequencies (cm^{-1}), Infrared Intensities (km/mol, in Parentheses) and Bond Lengths (Å) Calculated for PdH and Pd(H_2) Using Density Functional Theory[a]

functional, basis, pseudopotential	PdH, $^2\Sigma^+$	Pd(H_2), $^1A_1$
B3LYP	2014 (111)	
6-311++G(2d,2p)	1413 (56)[b]	995.7 (170) a_1, 1444.3 (8) b_2, 2935.5 (82) a_1[c]
SDD	1.541	PdH, 1.698; HH, 0.854
B3LYP	2011 (109)	
6-311+G(2d, 2p)	1429 (55)	1006 (171), 1450 (8), 2939 (82)
SDD	1.542	1.697, 0.854
B3LYP	2024 (111)	
6-311+G(d,p)	1439 (56)[b]	1011 (177), 1470 (10), 2914 (83)[d]
SDD	1.540	1.691, 0.858
BPW91	2033 (166)	
6-311+G(2d,2p)	1445 (84)[b]	863 (119), 1194 (11), 3032 (137)
LANL2DZ	1.531	1.763, 0.838
BPW91	2069 (108)	
6-311+G(d,p)	1470 (55)[b]	896 (151), 1416 (16), 2472 (94)[e]
LANL2DZ	1.530	1.692, 0.909

[a] These calculations predict H_2 bond length (0.743 Å) and harmonic frequency (4417 cm^{-1}). [b] For PdD, experimental data $\omega = 1446$ cm^{-1}, $\nu = 1407$ cm^{-1}, and $r_e = 1.528$ Å.[38] [c] Pd−η^2-H_2 complex, 17.5 kcal/mol more stable than Pd + H_2. Dipole moment, 1.06 D. Frequencies and intensities for Pd(HD) are 797.8 (96), 1276.2 (40), and 2552.3 (61) and for Pd(D_2) are 710.5 (87), 1022.3 (4), and 2077.5 (41). [d] Pd−H_2 bond length and a_1 Pd−H_2 frequency for C_{2v} G--Pd(H_2) complexes: Ne, 1.687 Å, 1022 cm^{-1} (171 km/mol); Ar, 1.684, 1051 (194); Kr, 1.691, 1057 (224); Xe using SDD, 1.706, 1038 (256). [e] For comparison Pd(H_2)$^+$, $^2A_1$, gives 1.849 and 0.796 Å bond lengths and 752 (19), 1123 (27), and 3683 (31) frequencies and is 192.5 kcal/mol higher than Pd(H_2), $^1A_1$, at this level of theory.

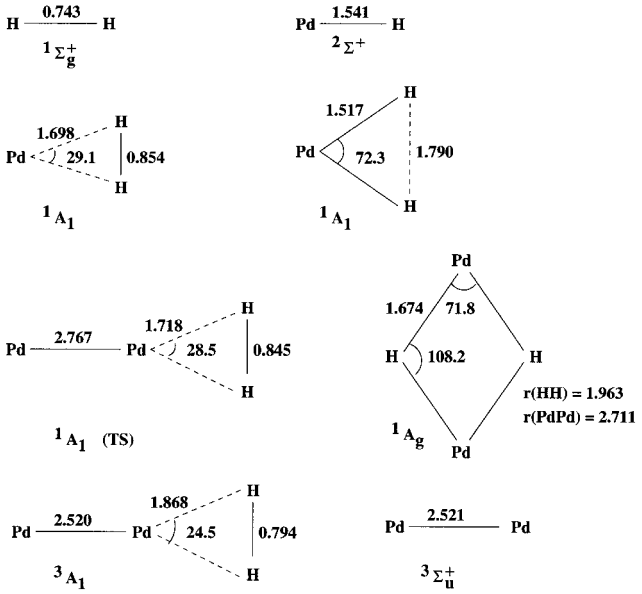

Figure 10. Structures calculated for the Pd−H_2 system. Angles are in deg, and distances, in angstroms.

± 10 cm^{-1}; PdD fundamental 1406.8 cm^{-1}),[38,39] and the SDD pseudopotential produces a better fit as does the B3LYP functional. The basis sets with diffuse functions (+ and ++) give almost the same frequencies for PdH and Pd(H_2) (Table 3). The harmonic frequency calculated for H_2 (4417 cm^{-1}) is in excellent agreement with the 4401.2 cm^{-1} observed value.[38] Because polarization effects in these complexes, which involve electrostatic interactions, are very important, most of the reported calculations use the ++ basis set, the B3LYP functional, and the SDD pseudopotential. Figure 10 shows the calculated Pd(H_2) structure. The end-bonded PdHH complex is computed to be an inversion transition state with an imaginary bending frequency.[24] In addition, calculations were done for the G−Pd(H_2) complexes for G = Ne, Ar, Kr, and Xe at the B3LYP/6-311+G(d,p)/SDD level, and relevant parameters are given in Table 3.

Calculations were done for the Pd$(H_2)_2$ complex starting with a planar structure and equal bonds, but this structure had two imaginary frequencies. The energy was lowered slightly by allowing all Pd--H bonds to converge independently, but one imaginary frequency remained using the larger ++ basis set in the planar configuration (with the smaller + basis set no imaginary frequency was found for the distorted planar structure). An almost D_{2d} structure with slightly unequal Pd--H bonds is a local minimum; the calculated frequencies are listed in Table 4. The D_{2d} structure, shown in Figure 11, is 0.4 kcal/mol lower in energy, and the frequencies change only slightly (Table 4). The spectra to be assigned below suggest that the two dihydrogen subunits may be slightly nonequivalent, which, of course, could be due to a matrix effect.

DFT calculations performed for Pd$(H_2)_3$ using both basis sets failed to converge for the D_{3h} structure. A calculation using the ++ set in C_{2v} symmetry (same Pd--H bond lengths for two H_2 subunits but different for the third H_2 subunit) converged (bond lengths 1.7964 and 1.7966 Å, H−H = 0.8223 Å) and a calculation using the + set in C_{3h} symmetry (unequal Pd--H in each H_2 but the same for three H_2) converged (bond lengths 1.7939 and 1.7943 Å, H−H = 0.8239 Å), giving essentially the same frequencies, which are listed in Table 5, along with the HD and D_2 substituted frequencies for the former calculation. It appears that Pd$(H_2)_3$ is effectively a trigonal planar complex; note the small calculated separations in the strong in-plane bending frequencies (0.7 cm^{-1}) and the antisymmetric Pd−H_2 and H−H stretching frequencies (0.2 and 1.9 cm^{-1}), which are degenerate in D_{3h} symmetry. A calculation starting with three out-of-plane H_2 molecules converged to the planar structure. Finally, calculations for Pd$(H_2)_4$ failed to converge, and there is no experimental evidence for this species.

Calculations were done for Pd_2H_2 on the singlet and triplet surfaces. The planar singlet complex Pd--Pd(H_2) is bound by 9.2 kcal/mol, but this structure is a transition state with one imaginary out-of-plane frequency involving the complexing Pd atom going over to the planar, rhombic $(PdH)_2$ structure, which is a global minimum (Figure 10). With the smaller + set, and in previous calculations,[14,24] a nonplanar cyclic structure was converged. Clearly, the diffuse function is important. The triplet Pd--Pd(H_2) complex is 38.5 kcal/mol more stable than Pd_2 + H_2, 10.0 kcal/mol more stable than Pd + Pd(H_2), but 31.1 kcal/

TABLE 4: Frequencies (cm^{-1}), Infrared Intensities (km/mol, in Parentheses), and Bond Lengths (Å) Calculated for $Pd(H_2)_2$

almost D_{2d}[a]	D_{2d} $Pd(H_2)_2$[b]	$Pd(H_2)(D_2)$	$Pd(HD)_2$	$Pd(D_2)_2$
210.3 (3)	251.7 (6) e	217.7 (2) b_2	205.8 (2) a	1181.1 (2) e
252.2 (4)	535.0 (0) b_1	220.0 (2) b_1	212.6 (2) b	378.4(0) b_1
507.4 (1)	903.8 (397) b_2	462.9 (0) a_2	466.5 (0.2) a	650.7 (206) b_2
890.0 (384)	1091.4 (0) a_1	692.1 (174) a_1	730.3 (236) b	772.0 (0) a_1
1077.6 (2)	1412.1 (1) e	1000.0 (0.3) b_2	850.7 (0.1) a	999.7 (0.5) e
1392.2 (5)	3280.2 (0) a_1	1017.1 (128) a_1	1245.6 (70) b	2320.3 (0) a_1
1401.5 (0)	3300.0 (159) b_2	1411.8 (0.5) b_1	1280.1 (0.2) a	2335.4 (78) b_2
3286.9 (2)		2328.0 (36) a_1	2846.4 (0.1) a	
3303.9 (180)		3290.0 (82) a_1	2864.7 (115) b	

[a] Bond lengths: 1.750, 1.753, 0.822, 1.741, 1.764, 0.821 Å. [b] Bond lengths: 1.749, 0.822 Å.

TABLE 5: Frequencies (cm^{-1}) and Infrared Intensities (km/mol, in Parentheses) Calculated for $Pd(H_2)_3$

$Pd(H_2)_3$[a]	$Pd(H_2)_2(D_2)$	$Pd(H_2)(D_2)_2$	$Pd(D_2)_3$	$Pd(HD)_3$	$Pd(HD)_2(DH)$	$Pd(H_2)_3$[b]
328.8 (44) a_1	272.3 (29)	237.6 (22)	236.6 (22)	270.3 (29)	266.0 (30)	337.5 (50)
329.5 (44) b_2	324.2 (46)	292.9 (1)	237.1 (23)	270.9 (30)	275.8 (29)	341.6 (50)
363.1 (2) b_1	328.9 (0)	298.1 (39)	263.7 (1)	285.3 (0.9)	281.5 (0.8)	371.3 (2)
443.0 (0) b_1	331.6 (1)	326.1 (0.3)	313.4 (0)	383.5 (0)	369.5 (0.1)	448.3 (0)
444.8 (0) a_2	440.0 (0)	329.8 (0)	314.7 (0)	385.2 (0)	471.3 (0.4)	451.2 (0)
484.1 (0) a_2	471.1 (0)	457.9 (0)	342.4 (0)	441.7 (0.4)	426.6 (0.1)	491.3 (0)
827.9 (95) a_1	626.9 (32)	603.9 (41)	590.8 (50)	670.0 (58)	633.1 (60)	823.4 (89)
828.1 (95) b_2	794.9 (89)	635.0 (36)	590.9 (50)	670.1 (58)	697.5 (49)	825.1 (89)
958.9 (0) a_1	921.8 (24)	847.0 (41)	678.3 (0)	749.1 (0)	770.2 (4)	955.5 (0)
1269.8 (0) b_2	964.1 (12)	914.9 (0.1)	898.2 (0)	1148.3 (0)	1101.6 (26)	1278.6 (0)
1345.8 (1) a_1	1297.9 (0.1)	990.3 (9)	952.1 (0.4)	1181.2 (19)	1164.9 (8)	1356.3 (1)
1346.4 (1) b_2	1337.8 (3)	1314.4 (4)	952.5 (0.4)	1181.8 (19)	1232.7 (5)	1356.6 (1)
3253.8 (202) a_1	2308.4 (67)	2304.0 (99)	2302.4 (100)	2825.8 (151)	2815.5 (174)	3249.4 (206)
3255.7 (202) b_2	3255.5 (202)	2316.4 (35)	2303.1 (100	2827.4 (151)	2832.6 (125)	3249.6 (205)
3283.0 (0) a_1	3274.6 (66)	3262.4 (134)	2322.3 (0.2)	2846.9 (0.4)	2851.7 (4)	3279.5(0)

[a] C_{2v} symmetry, ++ basis set ; Pd−H, 1.7964, 1.7966 Å; H−H, 0.822 Å. [b] C_{3h} symmetry, + basis set; Pd−H, 1.739, 1.743 Å; H−H, 0.824 Å.

TABLE 6: Frequencies (cm^{-1}) and Infrared Intensities (km/mol, in Parentheses) Calculated for Three Pd_2H_2 Structures Using B3LYP/6-311++G(2d,2p)/SDD

Pd--$Pd(H_2)$, C_{2v}[a]	$Pd(H_2)Pd$, D_{2d}[b]	Pd--$Pd(H_2)$, C_{2v}[c]
154.4 i (6) b_1	160.9 (55) b_{1u}[d]	200.4 (0) b_1
74.1 (2) b_2	199.0 (0) a_g	216.9 (6) b_2
119.5 (0) a_1	1224.8 (0) b_{3g}	223.9 (5) a_1
947.1 (611) a_1	1269.5 (107) b_{3u}	704.3 (22) a_1
1413.1 (3) b_2	1353.0 (280) b_{2u}	1095.2 (6) b_2
3015.2 (143) a_1	1480.4 (0) a_g	3630.1 (113) a_1

[a] Singlet state, 9.2 kcal/mol more stable than Pd + $Pd(H_2)$. [b] Singlet state, 41.1 kcal/mol more stable than Pd + $Pd(H_2)$. [c] Triplet state, 38.5 kcal/mol more stable than Pd_2(triplet) + H_2 but 31.1 kcal/mol higher than singlet $Pd(H_2)Pd$. [d] Frequencies and intensities calculated for Pd(HD)Pd are 132.8 (41), 199.0 (0), 905.2 (44), 958.0 (43), 1294.6 (166), and 1394.8 (37) and for $Pd(D_2)Pd$ are 116.6 (28), 198.6 (0), 866.5 (0), 902.8 (54), 960.2 (141), and 1051.6 (0).

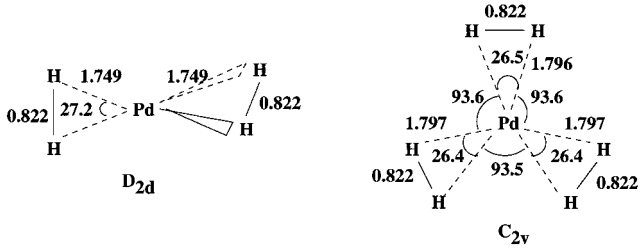

Figure 11. Structures calculated for $Pd(H_2)_2$ and $Pd(H_2)_3$. Angles are in deg, and distances, in angstroms.

mol less stable than singlet $(PdH)_2$. Frequencies calculated for three Pd_2H_2 species are given in Table 6.

DFT calculations were done for two isomers of PdH_3, namely the (H_2)--PdH complex and the open PdH_3 molecule, and the results are collected in Table 7. Similar calculations were done for the most stable $Pd(H_2)$ cation and anion isomers to assist in identifying the photosensitive band, and the important parameters are listed in Table 8 for two basis sets.

TABLE 7: Frequencies (cm^{-1}), Infrared Intensities (km/mol, in Parentheses), and Bond Lengths (Å) Calculated for (H_2)--PdH and PdH_3 Using B3LYP/6-311+G(d,p)/SDD[a]

(H_2)--PdH, $^2A_1$	PdH_3, ^2A
HH, 0.786; (H_2)−Pd, 1.890	two long PdH, 1.600
PdH, 1.567	one short PdH, 1.501
534 (12) b_1, 541 (18) b_2	large HPdH angle, 126.3°
721 (15) a_1, 1182 (4) b_2	other HPdH angle, 76.8°
1989.7 (99) a_1[b]	288 (107) a″, 456 (8) a′
3764 (48) a_1	676 (26) a′, 1656 (55) a″
	1917 (14) a′, 2274 (3) a′

[a] PdH_3 is 22.1 kcal/mol higher than $(H_2)PdH$. [b] Strong mode for (HD)PdH, 1988.9; (D_2)PdH, 1987.6; (H_2)PdD, 1415.7; (HD)PdD, 1414.8; and (D_2)PdD, 1413.0 cm^{-1}.

Discussion

Seven sets of new product absorptions will be assigned to palladium−hydrogen species on the basis of frequency shifts on HD and D_2 substitution and agreement with vibrational spectra calculated using DFT.

PdH. The strong, sharp 1952.8 cm^{-1} absorption was observed only in laser-ablation experiments where excess energy is available in the reagent metal atom.[40] This absorption shifted to 1403.5 cm^{-1} with D_2, and only these pure isotopic features were observed using HD. The 1952.8/1403.5 = 1.391 H/D frequency ratio is characteristic of heavy-metal hydrides involving the mostly harmonic potential associated with strong bonding. Sharp, weak 1961.9 and 1958.5 cm^{-1} neon matrix bands, which shifted to 1409.8 and 1406.3 cm^{-1} with deuterium, are appropriate for PdH and PdD. The 1952.8 and 1403.5 cm^{-1} argon matrix and 1961.9 and 1409.8 cm^{-1} neon matrix absorptions are in excellent agreement with gas-phase measurements

TABLE 8: Frequencies (cm^{-1}), Infrared Intensities (km/mol, in Parentheses), and Bond Lengths (Å) Calculated for $Pd(H_2)^+$ and PdH_2^- Using B3LYP and SDD

ion	6-311+G(d, p)	6-311++G(2d, 2p)
$Pd(H_2)^+$	PdH, 1.821; HH, 0.804	PdH, 1.824; HH, 0.803
$^2A_1$[a]	862 (25) a_1, 1282 (18) b_2, 3574 (28) a_1	861 (28), 1267 (18), 3572 (27)
$Pd(H_2)^-$	PdH, 1.702; HH, 0.865	
$^2A_1$[b]	945 (21) a_1, 1251 (218) b_2, 2808 (121) a_1	
$HPdH^-$	PdH, 1.695; HPdH, 180°	PdH, 1.698; HPdH, 180°
$^2\Sigma_g^+$[c]	693.4 (105) π_u, 1313.3 (2667) σ_u, 1672.7(0) σ_g	690.1 (120), 1304.1 (2799), 1662.2 (0)
PdH_2^-	PdH, 1.632; HPdH, 125.5°	PdH, 1.633; HPdH, 125.7°
$^2B_2$[d]	596 (120) a_1, 1527 (371) b_2, 1710 (201) a_1	599 (131), 1514 (430), 1697 (221)

[a] The $^2A_1$ cation is 198.3 and 198.1 kcal/mol above $^1A_1$ $Pd(H_2)$ with the 6-311+G(d,p) and 6-311++G(2d, 2p) basis sets, respectively. [b] The $^2A_1$ anion is 8.6 kcal/mol below $^1A_1$ $Pd(H_2)$ with 6-311+G(d,p). [c] The $^2\Sigma_g^+$ anion is 13.4 and 13.3 kcal/mol below $^1A_1$ $Pd(H_2)$ with the 6-311+G(d,p) and 6-311++G(2d, 2p) basis sets, respectively. The stretching modes calculated for $HPdD^-$ are 1013.1 (1249) and 1540.9 (754) and for $DPdD^-$ are 937.6 (1338) and 1183.2 (0) with the 6-311+G(d,p) basis, and those for $HPdD^-$ are 1006.2 (1313) and 1531.0 (790) and for $DPdD^-$ are 931.0 (1405) and 1175.8 (0) for 6-311++G(2d, 2p) [d] The $^2B_2$ anion is 13.6 kcal/mol below $^1A_1$ $Pd(H_2)$ with the 6-311+G(d,p) and 6-311++G(2d, 2p) baisis sets.

of the PdH and PdD fundamentals (1945 ± 10 and 1406.8 cm^{-1}, respectively),[38,39] and the DFT calculated harmonic frequencies (Table 3) are slightly higher as expected (scale factors (observed/calculated ++set) for PdH and PdD are 0.970 and 0.993). Accordingly, the 1952.8 and 1961.9, 1958.5 cm^{-1} absorptions are assigned to PdH in solid argon and neon.

The direct reaction with H_2 is calculated to be endothermic, but excess energy in the laser-ablated metal[40] atoms makes reaction 1 possible during the condensation process. On the other hand weak absorptions detected for Ar_nH^+ and Ar_nD^+ verify that H and D atoms are produced in the laser-ablation experiments. The marked growth of the PdH absorption on annealing, particularly in low concentration and 4 K codeposition experiments, shows that the direct atom reaction 2 is spontaneous in the cold argon matrix even though ground-state Pd is closed shell (d^{10}). This is consistent with the observation of $^2\Sigma^+$ PdH in ESR experiments using thermal Pd and H atoms and using laser-ablated Pd with molecular H_2.[41,42]

$$Pd + H_2 \rightarrow PdH + H \quad \Delta E = +52.3 \text{ kcal/mol} \qquad (1)$$

$$Pd(^1S) + H(^2S) \rightarrow PdH(^2\Sigma^+) \quad \Delta E = -57.8 \text{ kcal/mol} \qquad (2)$$

The weak 1900.8 cm^{-1} satellite of PdH (Figure 1) increases relative to the 1952.8 cm^{-1} band with increasing H_2 concentration and on 20 K annealing; the 1900.8 cm^{-1} band shifts to 1366.4 cm^{-1} with D_2 giving the same H/D = 1.391 ratio as PtH so a (H_2)--PdH complex is suggested. The small secondary displacements observed with HD (1899.0, 1368.2 cm^{-1}) and $H_2 + D_2$ (1987.9, 1369.2 cm^{-1}) show that the perturbing species contains hydrogen (deuterium). Our calculations find the (H_2)--PdH complex to be bound by 9.9 kcal/mol and to sustain a 34.5 cm^{-1} red shift in the strong Pd−H fundamental, in excellent agreement with the observed 52.0 cm^{-1} red shift. Furthermore, the small secondary displacements for (HD)--PtH, (D_2)--PtH, (H_2)−PtD, and (HD)--PtD are in excellent agreement with our DFT frequency calculations for these isotopic complexes. Finally, the higher energy PdH_3 isomer was not observed in these experiments.

A weak, broad 1831.7 cm^{-1} feature increases relative to the 1900.8 and 1952.8 cm^{-1} absorptions with increasing H_2 concentration, and a higher $(H_2)_x$--PdH complex is suggested. The band shifts to 1315.5 cm^{-1} with D_2 and gives the H/D ratio 1.392, essentially the same as PdH and (H_2)--PdH. The observation of a large secondary isotope effect with HD (1826.3 cm^{-1}) and two bands (1831.7 and 1825.4 cm^{-1}) with $H_2 + D_2$ provides evidence for two perturbing hydrogen molecules and suggests $x = 2$. In pure D_2 the only PdD species was observed at 1321.0 cm^{-1} ; however, with 10% HD or 5% H_2 in D_2 a new weaker band was obseved at 1830.4 cm^{-1} for $(D_2)_x$--PdH (H/D ratio 1.386). The D_2 matrix observations confirm the identification of $(D_2)_x$--PdD.

$Pd(H_2)$, Species A. The split 954.4, 950.0 cm^{-1} band (labeled A) was the strongest absorption in thermal-evaporation experiments. It increased 2-fold on +10 K annealing and then gave way to 778.0 and 730.1 cm^{-1} bands on higher (+20 to +30 K) temperature annealing of the argon matrix sample. The latter B and C bands were favored relative to A with increasing H_2 concentration (Figure 4). With $H_2 + D_2$ reagent mixtures, the B and C absorptions revealed evidence for mixed isotopic components, but the A band did not, which suggests that species A contains a single H_2 submolecule. Thermal and laser-ablation experiments with a 100-fold Pd concentration range change and 4% or 2% H_2 maintained constant relative A, B, C band intensities and thus provide evidence for a constant Pd atom content in these product species. Other associated fundamental vibrations and excellent agreement with the infrared spectrum predicted by DFT (Table 3) demonstrates that species A is Pd-(H_2), the Pd-η^2-H_2 side-bonded complex.

Weaker 2971.4, 2401.8, and 1507.5 cm^{-1} absorptions are associated with the strong 950.0 cm^{-1} band by common annealing and photolysis behavior. The bands are substantially decreased by 365 nm irradiation and restored by further annealing (Figure 5). Assignment of the strong 950.0 cm^{-1} and weak 1507.5 cm^{-1} bands to $\nu_2(a_1)$ and $\nu_3(b_2)$ of the side-bonded, isosceles triangular $Pd(H_2)$ structure are confirmed by the DFT calculated frequencies. Note that the low isotopic ratios on the ν_2 and ν_3 Pd−H_2 stretching modes (950.0/714.4 = 1.329 and 1507.5/1098.0 = 1.373) indicate substantial anharmonicity. This is hardly surprising in a relatively weakly bound species. Using the estimated DFT binding energy $D_e \approx 6100$ cm^{-1} and supposing a Morse-type potential along the Pd−H_2 reaction coordinate, a $\omega_2 = 1000$ cm^{-1} implies a X_{22} anharmonicity value near −40 cm^{-1}. As the method overestimates D_e, it likely represents a lower limit. An approximate treatment using the well-known Darling−Dennison relation and the observed isotope ratios suggest X_{22} values around −50 cm^{-1} for PdH_2 and about half for PdD_2. The weak band at 2401.8 cm^{-1} should be assigned to an overtone or a binary combination level. The $\nu_2 + \nu_3$ combination band (1507.5 + 950.0 = 2457.5) might be considered first, but several facts indicate that, in the upper wavenumber region, the situation is likely to be complicated by anharmonic resonance, and a transition of different symmetry will be considered later.

The 2971.4 cm^{-1} band in $Pd(H_2)$ lies in the important H−H stretching mode region. This value is in the range for $Cr(CO)_5$-(H_2) in liquid xenon (3030 cm^{-1}) and solid $W(CO)_3(PR_3)(H_2)$

(2690 cm^{-1})[2,5] but noticeably higher than in the latter compound although the $\nu_a(W(H_2))$ and $\nu_s(W(H_2))$ modes (1570, 953 cm^{-1}) and H/D ratios 1.387, 1.356 are very near the above values for $Pd(H_2)$. In PdD_2 two bands are observed in the upper region at 2169 and 1916 cm^{-1} with comparable intensities behaving equally with concentration and photolysis effects. Careful relative intensity measurements indicate a 1.3 intensity ratio in favor of the lower frequency component. A likely explanation is an anharmonic resonance between the $\upsilon_1 = 1$ first level of the D−D stretching motion and a combination or overtone of appropriate symmetry. Making the common assumption of a negligible intensity for the forbidden transition, it is possible to estimate resonance-corrected positions near 2020 cm^{-1} for the fundamental and 2060 cm^{-1} for the forbidden transition. For symmetry reasons the $\nu_2 + \nu_3$ combination can be ruled out, and $2\nu_3$ would give rise to similar resonances in PdH_2 and PdD_2. Using the above X_{22} estimates, a $3\nu_2$ position is calculated near 2000 cm^{-1} and could be a potential candidate. The corresponding transition in PdH_2 would be calculated near 2550 cm^{-1}. The 2971/2020 H/D isotopic ratio on ν_1 is larger than the expected harmonic oscillator value, which indicates that this mode is also likely affected by anharmonic resonance. A weaker residual resonance in $Pd(H_2)$ would offer a possible explanation for the relatively strong intensity of the 2402 cm^{-1} transition and the anomalous position of the 2971 cm^{-1} band. Note that, in Pd(HD), only one band is observed in the upper region and below the average between 2971 and 2020 cm^{-1}, unlike what is predicted at the harmonic level in the DFT frequency calculations: 2935, 2552, and 2077 for ν_1 in $Pd(H_2)$, Pd(HD), and PdD_2, repectively (Table 3). Tentatively, the resonance-corrected ν_1 transitions are thus estimated near 2780, 2330, and 2020 for the three isotopic species.

The lower frequency ν_2 and ν_3 modes in Pd(HD) are, on the other hand, well reproduced by the DFT force field: 1276 and 798 cm^{-1}, compared to 1305.6 and 804.1 cm^{-1} experimentally. Also, the $\nu_3(b_2)$ mode is predicted to be substantially weaker than the $\nu_2(a_1)$ mode but symmetry lowering in Pd(HD) modifies the balance between the Pd−H and Pd−D coordinates in the normal modes associated with ν_2 and ν_3. The relative intensities are predicted to change from 8/170 in PdH_2 to 40/96 in PdHD, in qualitative agreement with the change in observed ratios from 1/180 to 1/4.5 (Table 3, Figure 7).

Finally, the strong 950 cm^{-1} band for Pd−η^2-H_2 in solid argon is in good agreement with krypton and xenon matrix spectra,[17] but infrared bands assigned to Pd−η^1-H in solid krypton are in fact due to the $Pd(H_2)_{2,3}$ complexes that will be discussed next. No infrared bands were observed which could be assigned to the end-bonded complex.[17,20] The Pd−η^1-H_2 complex is an inversion transition state with an imaginary bending frequency in our calculations;[24] although linear Pd−HH is lower in energy[21,22,24] than Pd + H_2 (6.0 kcal/mol lower in our best calculation), this complex is a saddle point on the potential surface and Pd−HH will arrange to $Pd(H_2)$. Interaction with Pd favors the side-bonded orientation owing, in part, to the quadrupole moment of dihydrogen.

$Pd(H_2)_2$, Species B. The 778.0 and 730.1 cm^{-1} absorptions require more H_2 than $Pd(H_2)$ as Figure 4 clearly demonstrates. Our DFT calculations predict the strongest infrared bands at progressively lower frequencies for $Pd(H_2)_2$ and $Pd(H_2)_3$ (Tables 4 and 5) so the B and C bands must be considered for $Pd(H_2)_2$ and $Pd(H_2)_3$. Unfortunately, $Pd(H_2)_2$ does not exhibit a strong bending mode that definitively quantifies the H_2 content, as will be shown below for $Pd(H_2)_3$, species C, but the spectroscopic evidence supports the identification of species B as $Pd(H_2)_2$. First, the 778.0 and 585.7 cm^{-1} B bands with H_2 and D_2 exhibit a H/D ratio, 1.328, similar to that for species A, but in contrast to the A bands, blue satellites are observed at 844 and 624 cm^{-1} in mixed $H_2 + D_2$ experiments, which are appropriate for $Pd(H_2)(D_2)$. In the HD samples a new 1172.0 cm^{-1} species B band is observed owing to mode mixing on symmetry lowering. Furthermore the associated 3038 cm^{-1} band with H_2 shows a red satellite at 3034 cm^{-1} with $H_2 + D_2$.

The calculations demonstrate that $Pd(H_2)_2$ contains two side-bonded H_2 subunits and exhibits antisymmetric and symmetric combinations of the analogous modes $\nu_1(a_1)$ (i.e. ν_s) and $\nu_3(b_2)$ (i.e. ν_a) for $Pd(H_2)$. Therefore, the strongest infrared absorption of $Pd(H_2)_2$ is the antisymmetric combination of ν_s modes, b_2 in D_{2d} symmetry, and the other three modes are very weak. Recall, however, that the ν_a mode for Pd(HD) is much stronger due to mixing with the ν_s mode than for $Pd(H_2)$ and this is the case for $Pd(HD)_2$ as well; the 1172.0 cm^{-1} band is due to this symmetric combination of antisymmetric modes for $Pd(HD)_2$ (Figure 7). Our DFT calculation predicts the strong infrared band for $Pd(H_2)_2$ at 903.8 cm^{-1}, which is 16.2% too high compared to the observed 778.0 cm^{-1} band, but the observed isotopic pattern is in good agreement with calculated frequencies. The two bands observed for $Pd(HD)_2$ at 1172.6 and 649.6 cm^{-1} are 6.3 and 12.3% below the calculated values. Symmetry is lowered in the $Pd(H_2)(D_2)$ species and the calculated bands are much lower in intensity, but new bands at 844 and 624 cm^{-1} can be assigned to $Pd(H_2)(D_2)$. These bands are slightly broader than the pure isotopic 778.0 and 585.7 cm^{-1} bands, which suggests that the $Pd(H_2)_2$ species may be slightly distorted by the matrix.

The DFT calculations predict the antisymmetric ν(H−H) stretching for $Pd(H_2)_2$ at 3300 cm^{-1}, higher than this mode for $Pd(H_2)$ but only 8.6% higher than the 3038 cm^{-1} band observed for $Pd(H_2)_2$. Clear $Pd(HD)_2$ and $Pd(D_2)_2$ counterparts are observed at 2639 and 2160 cm^{-1} (Figure 9) with the H/D ratio 1.406, which is characteristic of a pure H−H vibration. The 778.0 and 3038 cm^{-1} bands are assigned to the bis complex $Pd(H_2)_2$.

$Pd(H_2)_3$, Species C. The 730.1 cm^{-1} band is associated with a 2-fold stronger 319.5 cm^{-1} band on increasing H_2 concentration and annealing. Fortunately, the mixed isotopic spectra demonstrate that the 319.5 cm^{-1} band involves three equivalent H_2 subunits, as shown in Figure 8. First, $H_2 + D_2$ mixtures reveal the pattern for a doubly degenerate mode, which is two new bands for the $(H_2)_2(D_2)$ species (316.5 and 269.5 cm^{-1}) and one new band (293.6 cm^{-1}) plus extra absorption at 236.6 cm^{-1} for the $(H_2)(D_2)_2$ isotopic complex. Our calculations (Table 5) predict the $Pd(H_2)_2(D_2)$ in-plane bending modes 5 and 57 cm^{-1} below this mode for $Pd(H_2)_3$ and the bending modes for $Pd(H_2)(D_2)_2$ 56 and 1 cm^{-1} above this mode for $Pd(D_2)_3$ in excellent agreement with the observed band separations. It is important to note that the $Pd(HD)_3$ complex retains double degeneracy *when all HD are oriented the same way in the molecular plane*, but when one HD is turned opposing the other two, this degeneracy is split. The three bands observed with HD confirm this model: the central band at 266.3 cm^{-1} due to $Pd(HD)_3$ has 2× intensity owing to the double degeneracy, and the 274.9 and 259.1 cm^{-1} bands with 3× intensity are due to the split degeneracy and 3/1 statistical weight of the $Pd(HD)_2$-(DH) species (Figure 8e). Our calculations show that lifting the degeneracy in the latter molecule results in bands 5 cm^{-1} higher and 5 cm^{-1} lower than the degenerate mode for the $Pd(HD)_3$ species, again in excellent agreement with the observed spectrum. This mixed isotopic pattern confirms the identification of $Pd(H_2)_3$. We note that the only Pd dihydrogen complex observed in pure D_2 is $Pd(D_2)_3$ at 556.5 cm^{-1}.

The C bands at 730.1 and 549.4 cm^{-1} show an H/D ratio of 1.329 following the pattern established for $Pd(H_2)_2$ and $Pd(H_2)$. Although our DFT calculations predicted the strong Pd−H_2 stretching mode 4.8% too high for $Pd(H_2)$, similar calculations (Tables 3 and 4) predict the antisymmetric combination of symmetric modes 16.2 and 13.4% too high for $Pd(H_2)_2$ and $Pd(H_2)_3$, respectively. The degenerate Pd−HD stretching mode at 587.7 cm^{-1} for $Pd(HD)_3$ (approximately described as an out-of-phase combination of the Pd−(HD) coordinates) also shows evidence of splitting at 618.3 and 585.9 cm^{-1}. Finally, one component of the weak antisymmetric Pd−(HD) stretching mode for $Pd(HD)_3$ was observed at 1105.5 cm^{-1}.

These same calculations give the out-of-phase ν(H−H) mode of $Pd(H_2)_3$ at 3255 or 45 cm^{-1} below the value predicted for $Pd(H_2)_2$, and no bands fall in this region. However, on final annealing a broad 2909 cm^{-1} feature appears in the 8% H_2 spectrum (Figure 5). In the 24% H_2 experiments a strong broad 2909 cm^{-1} band appears on sample deposition. The 16% HD and D_2 experiments contain similar broad 2545 and 2070 cm^{-1} features; in the $H_2 + D_2$ sample, the 2902 cm^{-1} band revealed a new 2897 cm^{-1} shoulder. These broad absorptions are probably due to $Pd(H_2)_3$, $Pd(HD)_3$, and $Pd(D_2)_3$. The 2909 cm^{-1} band is 12.5% below the DFT calculated value, and the H/D ratio, 1.405, is in accord with that for a H−H vibration.

Pd--Pd(H_2), Species D. The species D absorptions increase markedly on annealing and follow species A even to the blue splittings on the 950.0 and 922.8 cm^{-1} bands for A and D, respectively. Species D features are observed 10 cm^{-1} below the strong A bands for Pd(HD) and $Pd(D_2)$ and at 1297.8 cm^{-1} below the weaker Pd(HD) mode at 1305.6 cm^{-1}. The marked proportional growth of D bands on annealing and the complete destruction on visible photolysis in favor of species E bands ($(PdH)_2$; see below) strongly suggest a Pd--Pd(H_2) complex. Although the singlet Pd--Pd(H_2) species is a transition state with an imaginary bending frequency, it is 9.2 kcal/mol more stable than Pd and Pd(H_2), and the D frequencies are well described by the strongest infrared band calculated for the singlet Pd--Pd(H_2) species to be 49 cm^{-1} below the strongest Pd(H_2) band, which may be compared to the observed 27 cm^{-1} red shift. Furthermore, the infrared intensity of the Pd--(H_2) mode is enhanced 3-fold in the Pd--Pd(H_2) complex. Comparison of the three highest frequencies of singlet Pd--Pd(H_2) with those for Pd(H_2) shows a minor perturbation due to the second Pd atom. In contrast the stable triplet complex is calculated to have a weak Pd−(H_2) mode at 704 cm^{-1}, which is not appropriate for species D. In this case, the argon matrix can prevent the singlet Pd--Pd(H_2) complex from rearranging into the more stable rhombic Pd(H_2)Pd or $(PdH)_2$ ring. Hence the matrix in effect provides a local minimum for a structure that is calculated to be a transition state in the gas phase. However, on visible photoexcitation this D → E conversion is complete and species E bands increase.

$(PdH)_2$, Species E. The sharp species E band at 1347.7 cm^{-1} shifts to 950.2 cm^{-1} with D_2 giving a 1.418 ratio, much higher than H/D ratios for species A−C but near the PdH ratio (1952.8/1403.5 = 1.391). Hence, the cohesion in species E involves similar bonding as PdH, in contrast to the electrostatic effects dominant in the $Pd(H_2)_{1,2,3}$ complexes. With HD a weak band at 1431.5 cm^{-1} and two strong bands at 1329.8 and 951.5 cm^{-1} are observed (Figure 6), which is appropriate for symmetry lowering. The combination band at 2722 cm^{-1} is due to the sum of the former two bands (1431.5 + 1329.8 = 2761.3), which verifies their assignments to the same product species. The E bands increase on annealing and on photodestruction of the D species using visible light. With Pd(HD)Pd, photolysis at 365 nm produces red satellite features at 1316.3 and 942.7 cm^{-1}, which give way on annealing to the stronger 1329.8 and 951.5 cm^{-1} absorptions of Pd(HD)Pd. All of this evidence is consistent with species E as $(PdH)_2$, and this assignment is supported by frequency calculations for the rhombic species (Table 6).

Agreement with B3LYP calculations for the b_{2u} mode is excellent, but the weaker b_{3u} mode is not observed either because of masking by CH_4 impurity or of less intensity than predicted by calculation. It is not uncommon for heavy-metal hydride $(MH)_2$ species to exhibit only one strong stretching mode.[43] Note that our calculation with the large 6-311++G(2d, 2p) basis set converged to the planar structure whereas an earlier DFT calculation using a smaller hydrogen basis sets found a slightly nonplanar structure.[14]

The broader 1395 and 1380 cm^{-1} bands appear to be related to species E. In fact these bands grow more on photolysis, Figure 4c,d, than the 1347.7 and 1342.4 cm^{-1} bands. The 1347.7 cm^{-1} band appears to increase more than the 1395 cm^{-1} band on annealing; one of these $(PdH)_2$ features may be the H_2 complex of the other. The observation of a single 952.6 cm^{-1} band with pure D_2 suggests that the lower features are complexed by dihydrogen.

Charged Species. The sharp 1247.0 cm^{-1} band, its HD-substituted components at 1479.5 and 981.8 cm^{-1}, and D_2 counterpart at 908.5 cm^{-1}, observed only with laser ablation, are reduced substantially by full-arc photolysis. These bands are favored relative to Pd(H_2) complexes by 4 K condensation and by using unusually low laser power, which also enhance the Ar_nH^+ and Ar_nD^+ absorptions. As laser ablation is known to also produce a minor yield of charged species (compare PdCO, $PdCO^+$, and $PdCO^-$ band absorbances),[26] the above bands must be considered for a charged PdH_2 species. The observation of only 1247.0 and 908.5 cm^{-1} bands with the $H_2 + D_2$ reaction suggests that a single H_2 molecule is involved in this ion product.[44]

The lowest energy $Pd(H_2)^+$ cation (by 2.8 eV) is determined to be a side-bonded $^1A_1$ complex by high level calculations,[42] so we computed frequencies for this cation (Table 8). The a_1 frequency calculated at 862 cm^{-1} is not appropriate for the observed 1247.0 cm^{-1} band nor is the calculated HD isotopic pattern near the observed 1479.5 and 981.8 cm^{-1} bands. Hence, the charged species observed here is not compatible with frequencies calculated for ground-state $Pd(H_2)^+$.

However, note the extremely high-intensity calculated for $^2\Sigma_g^+$ $HPdH^-$, which is near (0.2−0.3 kcal/mol above) the lowest ($^2B_2$) state at the B3LYP level of theory. Although the photosensitive 1247.0 cm^{-1} band could in principle be due to a cation or anion, the increase in relative intensity with *lower* laser power and *elimination* with CCl_4 additive, which preferentially captures the ablated electrons, confirm the anion identification.[26] Recall that the Ar_nD^+ yield was correspondingly increased with added CCl_4. Finally, the accurate reproduction of the observed H_2, HD, and D_2 isotopic product frequencies by DFT frequency calculations for $^2\Sigma_g^+$ $HPdH^-$ confirms this assignment and suggests that $^2\Sigma_g^+$ is actually the ground-state anion. Scale factors (observed/calculated ++ set) for the four frequencies are 0.956, 0.966, 0.976, and 0.976, respectively, which is the expected consistency for the slightly anharmonic vibration with H and D substitution.

Both bond stretching modes are allowed in the lower symmetry $HPdD^-$ anion, and the integrated absorbances of the 1479.5 and 981.8 cm^{-1} bands, 0.0153 and 0.0286 au × cm^{-1},

are in excellent agreement with the relative calculated intensities, 790 and 1313 km/mol. Although the product yield is much less in the shorter neon matrix experiments, a 912.9 cm^{-1} band decreases on 6 K annealing and photolysis as does the stronger HD counterpart at 986.0 cm^{-1}. The small blue argon-to-neon shift for PdD_2^- is in line with other observations.[26,45]

Laser photoelectron spectroscopy has been done for a series of first-row transition metal hydride and dihydride anions.[46,47] The electron affinity measured for NiH_2 (1.934 eV)[46] is somewhat higher than the electron affinity predicted here (0.64 eV) for the $Pd(H_2)$ complex. Finally, solid-state palladium dihydride dianion complexes have been recently characterized.[48] These compounds consist of linear $(HPdH)^{2-}$ dianions surrounded by alkali metal cations. Slightly higher frequencies are observed for the solid-state dianion than for matrix isolated PdH_2^-.

Reactions in the Matrix. It is important to note that all bands in Table 1 (except PdH and PdH complexes and charged species) were observed on deposition of thermal Pd and molecular H_2, and they increased on annealing the matrix, which indicates favorable exothermic reactions. The following reactions occur (B3LYP energies calculated with ++ basis set):

$$Pd(^1S) + H_2(^1\Sigma_g^+) \rightarrow Pd(H_2)(^1A_1) \quad \Delta E = -17.5 \text{ kcal/mol} \tag{3}$$

$$Pd + Pd(H_2) \rightarrow Pd\text{--}Pd(H_2)(^1A_1, TS) \quad \Delta E = -9.2 \text{ kcal/mol} \tag{4}$$

$$Pd(H_2) + Pd \rightarrow Pd(H_2)Pd(^1A_g) \quad \Delta E = -41.1 \text{ kcal/mol} \tag{5}$$

$$H_2 + Pd(H_2) \rightarrow Pd(H_2)_2(^1A_1, D_{2d}) \quad \Delta E = -18.1 \text{ kcal/mol} \tag{6}$$

$$H_2 + Pd(H_2) \rightarrow Pd(H_2)_3(^1A_1, C_{2v}) \quad \Delta E = -6.2 \text{ kcal/mol} \tag{7}$$

The palladium dihydride molecule, PdH_2, is calculated to be physically stable but 5.0 kcal/mol higher in energy than $Pd(H_2)$.[24] No evidence was found here for PdH_2 on the basis of calculated frequencies near 2000 cm^{-1}. If formed, PdH_2 relaxes to the more stable $Pd(H_2)$ complex in the matrix cage. Likewise the higher energy PdH_3 species was not observed. However, the hydrogen complex with PdH increased on annealing.

$$H_2 + PdH \rightarrow (H_2)\text{--}PdH \quad \Delta E = -9.9 \text{ kcal/mol (+ set)} \tag{8}$$

In addition to energetic Pd atoms, which make the endothermic hydrogen abstraction reaction 1 possible, laser-ablation produces Pd^+ cations, electrons, and high energy radiation. The latter is responsible for photoionization to form Ar_nH^+ and Ar_nD^+ in these experiments and CO^+ in other investigations.[26] Although the Pd^+ reaction product $Pd(H_2)^+$ was not observed here, possibly owing to low oscillator strength, $Pd(H_2)^+$ has been observed in similar ESR experiments[42] and $PdCO^+$ in CO studies.[26] The linear $HPdH^-$ anion is probably formed here by direct electron capture reaction 9. The observation of only PdH_2^- and PdD_2^- in the $H_2 + D_2$ reaction shows that a single dihydrogen molecule is involved in the electron capture process. The PdH_2^- product *did not* increase on annealing so all ablated electrons are scavenged during the condensation process. We have no way to measure any possible activation energy requirement for reaction 9, which completely dissociates dihydrogen. However, the anion is 14.7 kcal/mol more stable than $Pd(H_2)$ at the B3LYP/6-311++G(2d, 2p)SDD level (including ZPE). If the stability of linear PdH_2^- is compared to the unobserved higher energy open PdH_2, the electron affinity of PdH_2 is estimated to be 20 kcal/mol.

$$Pd(H_2) + e^- \rightarrow HPdH^-(^2\Sigma_g^+) \tag{9}$$

The complementary neon matrix experiments show that the $Pd(H_2)_{1,2,3}$ complexes can also be prepared in solid neon, and some interesting matrix effects are revealed. Although higher initial H_2 concentrations increase the relative yield of the higher complexes, annealing the neon matrix samples did not show the product growth found in argon; this is probably due to the trapping of little unreacted H_2 in the neon matrix. The small blue shift from argon to neon for PdH (1952.8 to 1958.5 cm^{-1}) and for PdD (1403.5 to 1406.3 cm^{-1}) is typical.[45] These measurements are important for PdH as an accurate gas-phase PdH frequency is yet to be determined whereas the PdD gas-phase fundamental is 1406.8 cm^{-1}.[38,39] The strong $Pd(H_2)_{2,3}$ fundamentals exhibit 14.4 and 15.6 cm^{-1} blue shifts from argon to neon, which is also typical. However, the large red shift for $Pd(H_2)$ from argon to neon (950.0 to 871.8 cm^{-1}) is due to a special matrix effect on the bare Pd center in the $Pd-(H_2)$ stretching vibration, which also shifts in solid krypton,[17] 960 cm^{-1}, and xenon,[17] 894 cm^{-1}. These shifts are qualitatively in agreement with the G--$Pd(H_2)$ model DFT calculations, Table 3, which of course, involve only a single noble gas atom; perhaps the inclusion of additional G atoms around Pd would expand the effect. The lowest value calculated for the least interacting neon atom is in agreement with our observations.

Bonding in Palladium Hydrides. In addition to the NBO analysis published on the simplest complex,[24] $Pd(H_2)$, the bonding between Pd and H_2 units has been analyzed using the electron localization function (ELF) topological method[49] to avoid difficulties with orbital partitioning schemes in systems involving several transition metal centers. The ELF calculations were performed with the TopMoD package.[50] The topological description of the chemical bond proposed by Silvi and Savin relies upon the gradient field analysis of the electron localization function (ELF)[49] of Becke and Edgecombe.[51] The molecular space is partitioned into basins of attractors which have clear chemical significance. These are either core basins surrounding nuclei or valence basins. The valence basins are characterized by their synaptic order which is the number of core basins with which they share a common boundary. Accordingly, monosynaptic basins correspond to lone pair regions (labeled as $V(X)$ where X denotes the atom), whereas disynaptic ones correspond to bonding regions[52] (labeled as $V(X,Y)$, where X,Y denote the bonding atoms). For the $Pd(H_2)_{1,2,3}$ complexes the only existing disynaptic basins are those correponding to V(H,H), involving the H−H bond (Table 9), thus indicating no real onset of covalency in the Pd−H interaction. However, polysynaptic basins involving Pd atoms are found for the hydrides. The PdH monohydride has one and the metastable HPdH neutral and the $HPdH^-$ anion have two V(Pd,H) disynaptic basins corresponding to Pd−H single bonds but with reduced electron population for the neutral dihydride which is, in fact, unstable with respect to the $Pd(H_2)$ complex The PdH monohydride also forms a stable $HPd(H_2)$ complex. The stable rhombic $(PdH)_2$ ring structure also has two basins, but these involve trisynaptic basins V(Pd,H,Pd) characteristic of three-center−two-electron bonds, reponsible for the relative stability of the molecule. In this compound the second metal center is critical to the stability, as the V(Pd,H) electron population in the neutral dihydride structure appears too small to warrant stability. The extra electron in the dihydride

TABLE 9: Topological Population Analysis (in e) Obtained Using the ELF Function[a]

	V(H,H)	*V*(H,Pd)	*V*(Pd,Pd)	*q*(Pd)
Molecule				
H−H	2.00			
Complexes				
Pd−(H_2)	2.44			0.44
Pd−(H_2)$_2$	2.29 × 2			0.58
Pd−(H_2)$_3$	2.29 × 3			0.87
HPd−(H_2)	2.15	1.70		
PdPd−(H_2)	2.41		0.43	
Hydrides				
PdH		1.71		
HPdH		1.56 × 2		
$HPdH^-$		1.66 × 2		
($PdH)_2$		1.66 × 2[b]		

[a] See ref 49. [b] *V*(Pd,H,Pd) basin.

anion also provides a critical increase in the PdH basins and switches the relative energies of dihydride and complex anion structures.

The three Pd(H_2)$_{1,2,3}$ complexes are characterized by increasing electron population transfer from Pd to *V*(H,H). The 0.06e net charge-transfer calculated with the NBO analysis at the same level of theory for Pd(H_2)[24] is certainly misleading in regard to the calculated dipole moment (1.06 D). The results of the topological analysis show a substantial increase in the *V*(H,H) bond basin (0.4e) with no *V*(Pd,H) population, indicating a dominant d → σ^* charge transfer interaction. This effect is however partially offset in the total dipole moment by polarization effects on the Pd core, shifting the effective positive center-of-charge closer to the H_2 ligand. In the Pd(H_2)$_{2,3}$ complexes the ligand effects on the Pd charge are almost exactly additive, leading to an electron population depletion too close to unity to enable further coordination higher than a tris(dihydrogen) complex.

Conclusions

Palladium atoms react with H_2 on condensation in excess argon to form the side-bonded Pd(H_2) complex, which is identified by the effect of HD and D_2 substitution on the observed 2971.4, 1507.5, and 950.0 cm^{-1} fundamental frequencies and by excellent agreement with the results of B3LYP/6-311++G(2d,2p)/SDD calculations. The PdHH complex is an inversion transition state not trapped by the matrix.

The Pd(H_2) complex readily adds one and two more H_2 submolecules to form Pd(H_2)$_2$ and Pd(H_2)$_3$, which are predicted by DFT to have approximately D_{2d} and D_{3h} structures. The strongest infrared absorptions (Pd−(H_2) and H−H stretching modes) are predicted 1.2% low to 16.2% high by our calculations.

Bonding in the Pd(H_2)$_{1,2,3}$ complexes has been analyzed using the ELF topological method, which confirms the predominant charge-transfer nature of the Pd−H_2 interaction with a minor amount of charge reorganization on the metal center in the cooperatively coupled donor−acceptor delocalizations. It also provides an understanding of the coordination trends and limits in this series.

The Pd(H_2) complex reacts spontaneously with a second Pd atom to form, on one side, the singlet Pd--Pd(H_2) complex, which is a transition state stabilized by the argon matrix, and, on the other side, Pd(H_2)Pd, which is the rhombic ring ($PdH)_2$ with no H−H bond. Clearly, one Pd atom forms only a complex with H_2, but two Pd atoms dissociate H_2 in the open ring ($PdH)_2$ molecule. This, too, is in agreement with the present and earlier theoretical calculations,[14,22] and with the observation of a variation in rate constants for H_2 activation by Pd_n clusters as a function of cluster size and the ultimate dissociation of H_2 on the Pd metal surface.[53−55]

In addition, laser ablation produces energetic Pd atoms which also form PdH, electrons which are captured to give PdH_2^-, and radiation which ionizes H and yields Ar_nH^+ in the matrix cage. The $HPdH^-$ species characterized here contains dissociated dihydrogen and is related to the palladium dihydride dianion in solid-state Li_2PdH_2 and Na_2PdH_2.[48]

Finally, a comparison between Pd and Pt reactions with H_2 is appropriate. Platinum inserts to form the open PtH_2 dihydride molecule[56] whereas palladium adds to give the Pd(H_2) complex,[17,24] as predicted by theory.[14−16] Both PtH and PdH form complexes with H_2 and in pure D_2 give the common ($D_2)_x$--MD product; however, with a single H_2 molecule, PdH gives a distinct (H_2)--PdH complex whereas PtH forms PtH_3.[56]

Acknowledgment. This work was supported by CNRS Grant UMR 7075 and NSF Grants CHE97-00116 and CHE00-78836, the Université Pierre et Marie Curie for an invited Professorship, and the University of Virginia for a Sesquicentennial Associateship for L.A. We thank D. Carrére for assistance with the thermal experiments.

References and Notes

(1) Kubas, G. J. *Acc. Chem. Res.* **1988**, *21*, 120.
(2) Kubas, G. J.; Ryan, R. R.; Swanson, B. I.; Vergamini, P. J.; Wasserman, H. J. *J. Am. Chem. Soc.* **1984**, *106*, 451.
(3) Sweany, R. L. *J. Am. Chem. Soc.* **1985**, *107*, 2374.
(4) Upmacis, R. K.; Gadd, G. E.; Poliakoff, M.; Simpson, M. B.; Turner, J. J.; Whyman, R.; Simpson, A. F. *J. Chem. Soc.,Chem. Commun.* **1985**, *27*. Upmacis, R. K.; Poliakoff, M.; Turner, J. J. *J. Am. Chem. Soc.* **1986**, *108*, 3645.
(5) Morris, R. H.; Sawyer, J. F.; Shiralian, M.; Zubkowski, J. D. *J. Am. Chem. Soc.* **1985**, *107*, 5581. Crabtree, R. H.; Lavin, M. *J. Chem. Soc., Chem. Commun.* **1985**, 794.
(6) Collman, J. P.; Wagenknecht, P. S.; Hembre, R. T.; Lewis, N. S. *J. Am. Chem. Soc.* **1990**, *112*, 1294.
(7) Jackson, S. A.; Hodges, P. M.; Poliakoff, M.; Turner, J. J.; Grevels, F. W. *J. Am. Chem. Soc.* **1990**, *112*, 1221.
(8) Heinekey, D. M.; Oldham, W. J. *Chem. Rev.* **1993**, *93*, 913.
(9) Bender, B. R.; Kubas, G. J.; Jones, L. H.; Swanson, B. I.; Eckert, J.; Capps, K. B.; Hoff, C. D. *J. Am. Chem. Soc.* **1997**, *119*, 9179.
(10) Heitz, M.; Daniel, C. *J. Am. Chem. Soc.* **1997**, *119*, 8269.
(11) Chin, R. M.; Barrera, J.; Dubois, R. H.; Helberg, L. E.; Sabat, M.; Bartucz, T. Y.; Lough, A. J.; Morris, R. H.; Harman, W. D. *Inorg. Chem.* **1997**, *36*, 3553.
(12) Esteruelas, M. A.; Ore, L. A. *Chem. Rev.* **1998**, *98*, 577.
(13) Wang, X.; Andrews, L. *J. Phys. Chem. A* **2000**, *104*, 9892.
(14) Chi, Q.; Musaev, D. G.; Morokuma, K. *J. Chem. Phys.* **1998**, *108*, 8418.
(15) Balasubramanian, K. *J. Chem. Phys.* **1987**, *87*, 2800.
(16) Balasubramanian, K.; Feng, P. Y.; Liao, M. Z. *J. Chem. Phys.* **1988**, *88*, 6955 and references therein.
(17) Ozin, G. A.; Garcia-Prieto, J. *J. Am. Chem. Soc.* **1986**, *108*, 3099.
(18) Li, S.; Weiner, H. A.; Van Zee, R. J.; Weltner, W., Jr. *J. Chem. Phys.* **1997**, *106*, 2583.
(19) Low, J. J.; Goddard, W. A., III. *J. Am. Chem. Soc.* **1984**, *106*, 8321.
(20) Jarque, C.; Novaro, O.; Ruiz, M. E.; Garcia-Prieto, J. *J. Am. Chem. Soc.* **1986**, *108*, 3507. Novaro, O.; Jarque, C. *Theor. Chim. Acta* **1991**, *80*, 19.
(21) Backvall, J. E.; Bjorkman, E. E.; Petterson, L.; Siegbahn, P. E. M. *J. Am. Chem. Soc.* **1985**, *107*, 7265. Siegbahn, P. E. M. *Theor. Chim. Acta* **1994**, *81*, 441.
(22) Efremenko, I.; German, E. D.; Sheintuch, M. *J. Phys. Chem. A* **2000**, *104*, 8089.
(23) Dedieu, A. *Chem. Rev.* **2000**, *100*, 543.
(24) Andrews, L.; Manceron, L.; Alikhani, M. E.; Wang, X. *J. Am. Chem. Soc.* **2000**, *122*, 11011.
(25) Tremblay, B.; Manceron, L. *Chem. Phys.* **1999**, *250*, 187 and references therein.
(26) Liang, B.; Zhou, M. F.; Andrews, L. *J. Phys. Chem. A* **2000**, *104*, 3905 and references therein.
(27) Frisch, M. J.; Trucks, G. W.; Schlegel, H. B.; Scuseria, G. E.; Robb, M. A.; Cheeseman, J. R.; Zakrzewski, V. G.; Montgomery, J. A., Jr.; Stratmann, R. E.; Burant, J. C.; Dapprich, S.; Millam, J. M.; Daniels, A.

D.; Kudin, K. N.; Strain, M. C.; Farkas, O.; Tomasi, J.; Barone, V.; Cossi, M.; Cammi, R.; Mennucci, B.; Pomelli, C.; Adamo, C.; Clifford, S.; Ochterski, J.; Petersson, G. A.; Ayala, P. Y.; Cui, Q.; Morokuma, K.; Malick, D. K.; Rabuck, A. D.; Raghavachari, K.; Foresman, J. B.; Cioslowski, J.; Ortiz, J. V.; Baboul, A. G.; Stefanov, B. B.; Liu, G.; Liashenko, A.; Piskorz, P.; Komaromi, I.; Gomperts, R.; Martin, R. L.; Fox, D. J.; Keith, T.; Al-Laham, M. A.; Peng, C. Y.; Nanayakkara, A.; Gonzalez, C.; Challacombe, M.; Gill, P. M. W.; Johnson, B.; Chen, W.; Wong, M. W.; Andres, J. L.; Gonzalez, C.; Head-Gordon, M.; Replogle, E. S. ; Pople, J. A. *Gaussian 98, Revision A.7* ; Gaussian, Inc.: Pittsburgh, PA, 1998.

(28) (a) Becke, A. D. *J. Chem. Phys.* **1993**, *98*, 5648. (b) Lee, C.; Yang, W.; Parr, R. G. *Phys. Rev. B* **1988**, *37*, 785.

(29) (a) Becke, A. D. *Phys. Rev. A* **1988**, *38*, 3098. (b) Perdew, J. P.; Wang, Y. *Phys. Rev. B* **1992**, *45*, 13244.

(30) (a) Krishnan, R.; Binkley, J. S.; Seeger, R.; Pople, J. A. *J. Chem. Phys.* **1980**, *72*, 650. (b) Frisch, M. J.; Pople, J. A.; Binkley, J. S. *J. Chem. Phys.* **1984**, *80*, 3265.

(31) (a) Wadt, W. R.; Hay, P. J. *J. Chem. Phys.* **1985**, *82*, 284. (b) Hay, P. J.; Wadt, W. R. *J. Chem. Phys.* **1985**, *82*, 299.

(32) Andrae, D.; Haussermann, U.; Dolg, M.; Stoll, H.; Preuss, H. *Theor. Chim. Acta* **1990**, *77*, 123.

(33) Milligan, D. E.; Jacox, M. E. *J. Mol. Spectrosc.* **1973**, *46*, 460.

(34) Andrews, L.; Ault, B. S.; Grzybowski, J. M.; Allen, R. O. *J. Chem. Phys.* **1975**, *62*, 2461.

(35) Huber, H.; Kundig, E. P.; Moskovits, M.; Ozin, G. A. *J. Am. Chem. Soc.* **1973**, *95*, 332.

(36) Huber, H.; Klotzbucher, W.; Ozin, G. A.; Vandervoet, A. *Can. J. Chem.* **1973**, *51*, 2722.

(37) Moroz, A.; Sweany, R. L.; Whittenburg, S. L. *J. Phys. Chem.* **1990**, *94*, 1352 and references therein.

(38) Huber, K. P.; Herzberg, G. *Constants of Diatomic Molcules* ; Van Nostrand Reinhold: New York, 1979.

(39) McCarthy, M. C.; Field, R. W. *J. Chem. Phys.* **1994**, *100*, 6347.

(40) Kang, H.; Beauchamp, J. L. *J. Phys. Chem.* **1985**, *89*, 3364.

(41) Knight, L. B., Jr.; Weltner, W., Jr. *J. Mol. Spectrosc.* **1971**, *40*, 317.

(42) Knight, L. B., Jr.; Cobranchi, S. T.; Herlong, J.; Kirk, T.; Balasubramanian, K.; Das, K. K. *J. Chem. Phys.* **1990**, *92*, 2721.

(43) See for example: Souter, P. F.; Kushto, G. P.; Andrews, L.; Neurock, M. *J. Am. Chem. Soc.* **1997**, *119*, 1682.

(44) The $H_2 + D_2$ experiment produced a small amount of Pd(HD) due to H and D recombination and a weak corresponding $HPdD^-$ absorption.

(45) Jacox, M. E. *Chem. Phys.* **1994**, *189*, 149.

(46) Miller, A. E. S.; Feigerle, C. S.; Lineberger, W. C. *J. Chem. Phys.* **1986**, *84*, 4127.

(47) Miller, A. E. S.; Feigerle, C. S.; Lineberger, W. C. *J. Chem. Phys.* **1987**, *87*, 1549 and references therein.

(48) Olofsson-Martensson, M.; Haussermann, U.; Tomkinson, J.; Noreus, D. *J. Am. Chem. Soc.* **2000**, *122*, 6960 and references therein.

(49) Silvi, B.; Savin, A. *Nature* **1994**, *371*, 683.

(50) Noury, S.; Krokidis, X.; Fuster, F.; Silvi, B. *Comput. Chem.* **1999**, *23*, 597.

(51) Becke, A. D.; Edgecombe, K. E. *J. Chem. Phys.* **1990**, *92*, 5397.

(52) Berski, S.; Silvi, B.; Latajka, Z.; Leszynski, J. *J. Chem. Phys.* **1999**, *111*, 2542.

(53) Fayet, P.; Kaldor, A.; Cox, D. M. *J. Chem. Phys.* **1990**, *92*, 254.

(54) Gross, A.; Wielke, S.; Scheffler, M. *Phys. Rev. Lett.* **1995**, *75*, 2718.

(55) Gostern, M.; Sitz, G. O. *J. Chem. Phys.* **1997**, *106*, 7378.

(56) Andrews, L.; Wang, X.; Manceron, L. *J. Chem. Phys.* **2001**, in press. ($Pt + H_2$).